High Ambipolar Mobility in a Neutral Radical Gold Dithiolene Complex

DOI: 10.1002/ ((please add manuscript number))
Article type: Full Paper

High ambipolar mobility in a neutral radical gold dithiolene complex

*Asato Mizuno,[a‡] Helen Benjamin,[b‡] Yasuhiro Shimizu,[c] Yoshiaki Shuku,[a] Michio M. Matsushita,[a] Neil Robertson,[*b] and Kunio Awaga[*a]*

[a] Department of Chemistry & Integrated Research Consortium on Chemical Sciences (IRCCS), Nagoya University, Furo-cho, Chikusa-Ku, Nagoya 464-8602, Japan;
[b] EaStCHEM School of Chemistry, The University of Edinburgh, King's Buildings, David Brewster Road, Edinburgh, EH9 3FJ, UK;
[c] Department of Physics, Nagoya University, Furo-cho, Chikusa-Ku, Nagoya 464-8602, Japan
E-mail: awaga@mbox.chem.nagoya-u.ac.jp, neil.robertson@ed.ac.uk

Keywords: ((charge transport, field-effect transistors, organic semiconductors, dithiolene ligands, gold))

Abstract A new anionic gold dithiolene complex **NBu$_4$·[1]** has been synthesised from the (1-((1,1-biphenyl)-4-yl-)-ethylene-1,2-dithiolene ligand **1**, and the *cis* and *trans* isomers separated by recrystallization. The *trans* isomer is oxidised via electrocrystallisation to the neutral gold dithiolene complex **2**. Complex **2** crystallises in one-dimensional chains, held together by short (3.30-3.37 Å) S-S contacts, which are packed in a herringbone arrangement in the *ab*-plane. The complex exhibits semiconductor behaviour (σ_{RT} = 1.5 × 10^{-4} S cm^{-1}) at room temperature with a small activation energy (E_a = 0.11 eV), with greater conductivity along the stacking direction. The charge transport behaviour of complex **2** was further investigated in single crystal FET measurements, the first such measurements reported for gold dithiolene complexes. Complex **2** showed incredibly balanced ambipolar behaviour in the SC-FET, with high charge carrier mobilities of 0.078 cm^2 V^{-1} s^{-1}, the highest ambipolar mobilities reported for metal dithiolene complexes. This well-balanced behaviour, along with the activated conductivity and band structure calculations, suggests that **2** behaves as a Mott insulator. The magnetic properties were also studied by SQUID magnetometry and solid state ^{1}H NMR, with evidence of a non-magnetic ground state at low temperature.

1. Introduction

Metal dithiolene complexes have received a great deal of attention in recent years as potential molecular based functional materials, due to their high stability, magnetic, optical and conductive properties,

which can be tuned through variation of the metal centre or substitution pattern of the dithiolene ligands.[1–3] In particular, neutral nickel and gold bis(1,2-dithiolene) complexes have been studied as single component conductors,[2-18] due to attractive features such as their square planar geometry and delocalised electronic structure, which leads to favourable intermolecular stacking interactions (a requirement for solid state conductivity) and reversible and tuneable redox chemistry. Additionally, neutral gold dithiolene complexes can behave as Mott insulators, with one radical per site,[8,19–22] resulting in an activation barrier for conductivity behaviour that can be overcome with pressure.[16,23–25] Since the first molecular superconductor based on a metal dithiolene complex was reported, a charge transfer salt (TTF)$[Ni(dmit)_2]_2$,[26,27] a large number of neutral complexes containing dithiolene ligands with a TTF backbone have been synthesised,[3,18] such as $Au(ptdt)_2$,[10] and $Au(tmdt)_2$,[5,6,9,11,15,28,29] showing metallic or near metallic behaviour at ambient temperature and pressure. Neutral gold dithiolene complexes without TTF containing ligands have also been reported, such as $Au(\alpha\text{-}tpdt)_2$[30] and $Au(bdt)_2$[20,31–33], showing a wide variety of conductive properties, from semiconductor to metallic.[2,18,19,21,30,34–41] Several complexes in the thiazole dithiolate family have been reported showing activated conductivity under ambient conditions,[12,16,17,22,42,43] with some showing metal-like conductivity under pressure,[4,8,16] and one showing metallic behaviour under ambient conditions.[7]

Despite their favourable conductive properties, metal bis(dithiolene) complexes have been seldom studied for their field-effect transistor (FET) performance. Examples in the literature consist of a small number of nickel complexes that show moderate to high electron mobilities, with some complexes showing ambipolar behaviour although the carrier mobilities in these devices are not high.[44–46]

There are no reports in the literature of FET measurements on gold dithiolene complexes. In this work we present the synthesis, crystal structure, and electronic properties of new neutral gold radical complex **2**, containing the asymmetric (1-((1,1-biphenyl)-4-yl-)-ethylene-1,2-dithiolene ligand. Single crystal FET measurements were carried out to probe the charge carrier mobilities of **2**; these are the first FET measurements based on a gold dithiolene in the literature. **2** showed incredibly balanced ambipolar behaviour, with high charge carrier mobilities of 0.078 $cm^2\ V^{-1}\ s^{-1}$, comparable to the highest mobility

values reported for any metal complexes.[47,48] The ambipolar mobilities are also far higher than those for other metal complexes showing ambipolar behaviour.[44–46,49–52] **2** exhibits an activated conductivity behaviour with a very small activation energy (0.11 eV), attributed to the existence of a Mott insulating state based on the band calculations and FET measurements.

2. Results and Discussion

2.1. Synthesis and characterisation

As the dithiolone precursor is asymmetric, the anionic complex **NBu_4·[1]**, synthesised via the deprotection of the dithiolone, 4-(4-phenylphenyl)-1,3-dithiol-2-one, with sodium methoxide followed by addition of $KAuCl_4$ **(Scheme 1)**, is initially obtained as a mixture of the cis and trans isomers. The isomers can be distinguished by a 0.01 ppm difference between the dithiolene protons in the ^{1}H NMR, and the isomers do not appear to interconvert **(Figure S1)**. While rapid cis-trans isomerism in solution has been reported for asymmetric nickel dithiolene complexes,[53,54] rapid interconversion for asymmetric gold dithiolene complexes has not been observed.[4,7,8,12,16,17,33,39,40,42,43,55–57] In most cases, the isomers are separated after the oxidation to the neutral species by selective crystallisation of one isomer over the other. Here, after cation exchange with tetra-n-butylammonium iodide, we were able to separate the isomers of anion **NBu_4·[1]** via recrystallization to give the pure *trans* isomer in reasonable yield (45%), confirmed by ^{1}H NMR. The neutral complex **2** was then synthesised by galvanostatic electrocrystallisation; crystals grew at the anode on application of a 1.0 μA current to a solution of **NBu_4·[*trans*-1]** in a 0.1 M solution of $NBu_4 \cdot BF_4$ in DMF.

The UV-vis spectra **(Figure S2, Table S1)** of the anionic complex **NBu_4·[*trans*-1]** show intense ($\varepsilon >$ 10000 $dm^3\,mol^{-1}cm^{-1}$) bands below 400 nm, attributed to π-π* transitions on the ligand and ligand-to-metal charge transfer (LMCT) transitions. At higher concentrations, weak ($\varepsilon <$ 1000 $dm^3mol^{-1}cm^{-1}$) bands can be observed at 477 nm and 727 nm, likely corresponding to d-d transitions. On oxidation a band in the NIR (1462 nm) is observed; this has been observed previously for neutral gold radical complexes and has been assigned to either a SOMO-1 to SOMO transition,

or an intervalence charge transfer (IVCT) band of the form $[Au^{III}(L^{\bullet})(L)] \rightarrow [Au^{III}(L)(L^{\bullet})]$.[19,56,57]

Cyclic voltammetry measurements **(Figures S4,5 and Table S2)** on complex **NBu_4·[*trans*-1]** show one quasireversible oxidation and one quasireversible reduction at 0.03 and -1.98 V vs Fc/Fc^+, corresponding to the −1 to 0 oxidation and −1 to −2 reduction, respectively. The shape of the oxidation peak varies with scan rate and changes on subsequent scans; this is likely due to deposition of the insoluble neutral complex **2**, and a similar behaviour has been observed in other gold dithiolene complexes.[16,30,36,39,41]

Single crystals of **NBu_4·[*trans*-1]** and **2** suitable for X-Ray analysis were grown via slow diffusion of isopropanol into a solution in acetone and electrocrystallisation, respectively. The anion complex **NBu_4·[*trans*-1]** crystallises in the triclinic centrosymmetric space $P\bar{1}$ with two distinct anion (and cation) molecules in the asymmetric unit **(Figure S6, Table S3)**. The crystal structure confirms the square planar, trans geometry around the gold centre, and key bond lengths **(Table S4)** of the dithiolene moiety are in good agreement with those of other monoanionic gold complexes.[19,35,39,56] The asymmetric nature of the ligand is reflected in the difference in C-S bond lengths. No short S-S contacts are observed between the anionic complexes within the structure.

In contrast, the structure of neutral complex **2 (Figure 1)** shows significant S-S interactions. The complex crystallises in the monoclinic $P2_1/c$ space group, with one unique complex in the asymmetric unit. The geometry about the gold centres is square planar, with only a small distortion between the two S-Au-S planes (4.65 º). The complexes form a 1D regular chain along the *a* axis, and these 1D chains are packed in a herringbone manner in the *ab* plane. These herringbone structures are then aligned along the *c* axis. The short S-S contacts (< 3.70 Å) seen within the 1D chains are one of the shortest values among those of reported neutral gold dithiolene complexes.

In complexes with dithiolene ligands an important consideration is the “non-innocence” of the ligand.[58,59] In the case of the anion complex **NBu_4·[*trans*-1]**, the C-S and C-C bond lengths **(Table S4)** are consistent with the ene-1,2-dithiolate form of the dithiolene, suggesting that **NBu_4·[*trans*-1]** can be

described as a Au(III) bis(ene-1,2-dithiolate) complex, as has been proposed for other anionic gold dithiolene complexes.[19,39] On oxidation a slight shortening of the Au-S bond, a shortening of the C-S bond length, along with a slight lengthening in the C-C bond length is observed, indicating the adoption of a more dithioketone-like structure.[21,40] These bond changes suggest extensive delocalisation of the spin density over the dithiolene ligands, a conclusion that is supported by our computational work, and literature observations of other gold dithiolene complexes.[4,17,34,40,42,55]

2.2. Conductive properties

Electrical conductivity was measured on single crystals of **2** in the ab plane and along the *c* axis. The room temperature conductivity at ambient pressure for **2** in the *ab* plane, measured on multiple crystals, was in the range of 10^{-4}–10^{-5} S cm^{-1}, with a maximum value of 1.5×10^{-4} S cm^{-1}. A lower conductivity was observed along the *c*-axis (10^{-5}–10^{-6} S cm^{-1}), consistent with the dimensionality of the crystal structure, an observation that is reflected in the band calculations. Upon cooling, semiconductor behaviour is observed **(Figure 2)** in both the *ab* plane and along the *c* axis, with an activation energy of 0.11 eV. This is among the lowest activation energies reported for neutral gold dithiolene complexes that do not contain TTF moieties.[4,12,18] Heat capacity measurements **(Supporting Information, Figure S7)** supported the presence of a non-metallic state at low temperatures. The observed semiconductor behaviour, relatively low conductivity and uniform stacking in the solid state, along with the band calculations and FET behavior (vide infra), suggest that **2** can be described as a Mott insulator.

2.3. Magnetic properties

The temperature dependence of the magnetic susceptibility of **2 (Figure 3)** was measured with a SQUID magnetometer in the range 2-300 K, and corrected for sample diamagnetism. The susceptibility is almost temperature-independent from 300 to 60 K, then decreases down to 45 K, followed by a rapid increase approaching 0 K which is attributed to paramagnetic defects. The susceptibility (χ_p) of **2** is low, only 4×10^{-4} emu mol^{-1} at room temperature, far lower than expected for isolated S=1/2 molecules. This kind of Pauli-like, small paramagnetic susceptibility with weak temperature dependence is reported in other neutral gold dithiolene complexes with a thermally-activated conductivity.[4,5,12,16,17,22] The

decrease below 60 K could be ascribed to a transition to a non-magnetic ground state,[60] a suggestion supported by solid state ^{1}H NMR data, which show no critical divergence of T_1^{-1} and almost temperature independent signal shapes **(Figure S8)**, unlike that seen in antiferromagnetic transitions.[15,61] There was also no indication of a spin-flop transition as seen in antiferromagnets observed in the magnetization curves below 60 K. Low temperature X-ray diffraction data **(Figure S9, Table S5)** showed no clear indication of a structural phase transition. The temperature dependence of the electron paramagnetic resonance (EPR) signals displayed Curie-like behaviour **(Figure S10)**, consistent with the Curie-tail observed in the susceptibility measurements. Below 100 K, the peak-to-peak line widths and *g*-factors show an almost temperature-independent behaviour, with the values of 19 mT and 2.03, respectively. Above 100 K the intensity of the EPR signals was too low to be detected.

2.4. Band structure calculations

In order to further understand the conductive properties of **2**, extended Hückel theory (EHT) calculations were performed on the obtained crystal structure to determine the band structure, as has been performed previously for gold dithiolenes.[2,13,21,29,42] First, the singly occupied molecular orbital (SOMO), SOMO-1 and lowest unoccupied molecular orbital (LUMO) of the isolated molecule were computed at the geometry present in the crystal structure (**Figures S11-13**), and the SOMO is shown in **Figure 4**, along with the spin density distribution. The SOMO is heavily delocalized across the dithiolene and the phenyl rings of the ligand, with only a 3% contribution from the Au atom, which could explain the strong inter- molecular magnetic interactions in the solid state.[17,34,36] The intermolecular interactions considered in the Hückel calculation are shown in **Figure 5**. **Table 3** lists the calculated overlap integrals and transfer integrals. As interactions along the *c* axis were negligible, we only considered interaction in the *ab* plane in the calculation; the interactions within the chain (interaction a) is about approximately an order of magnitude smaller than the inter-chain interactions (b1 and b2). These interactions are comparable to those resulting from the 'brick wall' packing of fluorinated oxobenzene-bridged bis-1,2,3-dithiazolyl (FBBO) radicals;[24] in the case of **2** the interchain interactions (b1, b2) are not equal due to the herringbone packing of the chains. The band structure was

calculated by the tight-binding approximation, and is shown in **Figure 6**. Each band in the figure is the superposition of two bands, with the lower four bands corresponding to bands originating from the SOMO-1 interactions of the four molecules in the unit cell, and the higher four bands originating from the SOMO orbitals. Bands originating from the LUMO orbitals were at significantly higher energy (-9.04 eV) and thus are not shown here. The band structure shows significant dispersion for the SOMO bands along the a^* and b^* directions, which are approximately and exactly parallel with the a and b directions, respectively. This is consistent with the interactions within and between the chains in the ab plane. The lack of dispersion along Γ-Z is expected, a result of the omission of interactions between planes along the c axis. Due to the lack of dimerisation in the crystal structure the SOMO (and SOMO-1) bands are not split; large splitting of the SOMO bands has been being provided as the explanation for the band semiconductor behaviour in previous gold radical complexes.[18] The calculations instead predict a metallic character for **2**, at odds with the experimentally observed semiconductor behaviour, however extended Hückel theory does not take into account strong electron correlation so this is consistent with our Mott insulator interpretation.[24]

2.5. FET measurements

Single-crystal field-effect transistors (SC-FETs) were fabricated **(device fabrication shown in Figure 7)** to investigate the possibility of an insulator-metal transition and/or a band-like transport in **2**. At present, there are no reports of FET devices of gold dithiolene complexes. The temperature dependence of the transfer characteristics were measured from 300 to 250 K under vacuum at a source-drain voltage V_D of 1 V **(Figure 8)** and –1 V **(Figure S14)**, which showed identical behaviour except for the direction of the current. Here, the difference of the source-drain current ΔI_D is plotted (ΔI_D = (I_D at V_G)–(I_D at V_G = 0 V), V_G: gate voltage) for each transfer curve due to the relatively large off-currents, likely caused by the bulk conductivity.[68,69] The large off-current also results in relatively small on/off ratios **(see Figure S15(b))**.

The device shows well-balanced, ambipolar characteristics in the measured temperature range, which is characteristic of FETs based on Mott insulator systems.[68–70] The value of the field effect mobility μ at

300 K is estimated to be 0.078 $cm^2\ V^{-1}\ s^{-1}$ for both electrons and holes, which is among the highest values for electrons in the FETs based on metal-dithiolene complexes, and the highest reported for holes.[44–46,48,51,71–73]

Furthermore, the ambipolar behaviour is incredibly well-balanced, a behaviour that is still a rare example among metal complexes, including other types of molecular skeletons **(Table 4)**.[44,45,74–77,46–51,71,72] The activation energy E_a for the thermally-activated behaviour of the field effect mobility value is estimated to be 0.065 eV for both carriers. While electric-field-induced Mott transitions have been reported in organic crystal FET devices previously,[70] in this case higher doping concentrations would be necessary to induce a metal-insulator transition. It should be noted that this device also works under air without significant change in the performance.

The charge transport properties were also investigated theoretically; the intermolecular hopping carrier mobilities were calculated on the basis of Marcus theory.[78–81] The calculated parameters and intermolecular carrier mobilities along the directions of the intermolecular interactions are listed in **Table 5**.

In the calculations the dihedral angles between the dithiolene and benzene moieties and between the benzene moieties were restricted (**Tables S6-7**), as when allowed to freely optimise they became larger than 30°, a significant distortion from the geometry obtained in the crystal structure. The results of the calculations for the unrestricted geometries are listed in **Tables S8-10**.

While the theoretical values for the hopping mobilities are greater (Table 5) than those obtained experimentally (0.078 $cm^2\ V^{-1}\ s^{-1}$), it can be seen that the mobilities and reorganization energies for holes and electrons are comparable, in agreement with the observed ambipolar behaviour. This can be explained by the fact that electrons and holes would be injected into the same orbital (SOMO), resulting in similar reorganization energies for both charge carriers, which in turn leads to comparable mobilities. Due to the intrachain interactions (Figure 5, interaction a) being weaker than the interchain interactions (interactions b1 and b2), the calculated mobilities in this direction are significantly lower.

The calculations also support the experimentally obtained activation energy for the mobility of charge carriers (0.065 eV), as it falls between the calculated values of λ and $\lambda/4$ for electrons (0.113 eV and 0.028 eV, respectively) and holes(0.147 eV and 0.037 eV, respectively).

3. Conclusions

We have reported the synthesis of a new neutral gold dithiolene complex, **2**, and investigated its electronic and conductive properties through single crystal conductivity and FET measurements. The crystal structure of complex **2** shows the formation of chains held together by very short S-S contacts, which are packed in a herringbone arrangement, indicating strong intermolecular interactions which provide a mechanism for conductivity. Complex **2** showed incredibly balanced ambipolar behaviour in the SC-FET measurements, the first such measurements reported for gold dithiolene complexes, with high charge carrier mobilities of 0.078 $cm^2\ V^{-1}\ s^{-1}$. This, along with the activated conductivity behaviour suggest that **2** behaves as a Mott insulator.

4. Experimental Section

Materials, Synthesis and Characterization: All commercially available chemicals were used without further purification. Ligand precursor 4-(4-phenylphenyl)-1,3-dithiol-2-one was prepared as described in the literature.[82] Mass spectra (ESI) were recorded with a Xevo QTOF (Waters) high resolution, accurate mass tandem mass spectrometer equipped with Atmospheric Solids Analysis Probe (ASAP) and Bruker MicroToF 2. Elemental analyses were carried out by Stephen Boyer of the Science Centre, London Metropolitan University using a Carlo Erba CE1108 Elemental Analyser.

Complex NBu_4·[1] NaOMe (1.00 g, 18.51 mmol) was added to a stirred solution of 4-(4-phenylphenyl)-1,3-dithiol-2-one (1.00 g, 3.70 mmol) in methanol/THF (15/5 ml) that had been degassed for 15 min with bubbling nitrogen. The mixture was stirred at RT for 1 h. The reaction mixture was heated to 50 ºC and $KAuCl_4$ (0.70 g, 1.85 mmol) was added. The mixture was stirred at 50 ºC for 1 h before the solvent was removed *in vacuo*. The residue was redissolved in acetone (100 ml) and tetrabutylammonium iodide (0.68 g, 1.84 mmol) was added. The mixture was stirred at RT overnight

and the solvent was removed *in vacuo*. Water (50 ml) was added, and the solution was filtered. The solid was dried, washed with acetone and the filtrate collected. The solvent was removed and the solid dissolved in acetone (150 ml) and heated to reflux. Isopropanol (100 ml) was layered over the hot solution and the solution was left for 2 days. The crystals obtained were collected via filtration and washed with isopropanol to give dark brown crystals of the trans isomer of the gold TBA salt, **NBu_4·[*trans*-1]** (0.77 g, 45%); δ_H (500 MHz; CD_3CN; Me_4Si) 7.72 – 7.63 (8H, m), 7.59 – 7.52 (4H, m), 7.47 – 7.44 (4H, m), 7.39 – 7.30 (2H, m), 6.76 (2H, s), 3.11 – 3.03 (8H, m), 1.59 (8H, dq, J = 11.8, 7.8), 1.35 (8H, h, J = 7.4), 0.97 (12H, t, J = 7.4); MS(ESI, negative) calcd for $[C_{44}H_{56}AuNS_4]^-$ m/z = 681.0113, found 681.0139. Anal. calcd for $C_{44}H_{56}AuNS_4$: C, 57.19; H, 6.11; N, 1.52. Found: C, 57.18; H, 6.08; N, 1.64.

The filtrate was collected, and further isopropanol was added. Over time light brown crystals separated, **NBu_4·[*cis*-1]** (0.40 g, 23%); δ_H (500 MHz; CD_3CN; Me_4Si) 7.72 – 7.63 (8H, m), 7.59 – 7.52 (4H, m), 7.47 – 7.44 (4H, m), 7.39 – 7.30 (2H, m), 6.75 (2H, s), 3.11 – 3.03 (8H, m), 1.59 (8H, dq, J = 11.8, 7.8), 1.35 (8H, h, J = 7.4), 0.97 (12H, t, J = 7.4).

*Electrochemical Synthesis of **2**:* The synthesis and crystallization of **2** was carried out by galvanostatic electrocrystallization in a 0.1 M DMF (anhydrous, N_2 degassed) solution of NBu_4·BF_4, containing 1 mM **NBu_4·[*trans*-1]** (10 mg for 10 mL DMF) in the anode side. H-shaped glass cells equipped with a glass filter and two Pt electrodes, were purged by N_2 gas, and were used for the electrocrystallization. The black platelet crystals of the neutral gold complex of **2** were obtained by galvanostatic electrocrystallization on Pt electrodes under a constant current of 1.0 μA within two weeks (**Figure S16**). The obtained crystals were collected via filtration and washed with acetonitrile to give the trans isomer of the neutral gold radical (2.3 mg, 30%); SEM-EDX (**Figure S17**): calcd S/Au = 4, found S/Au = 4.2 (averaged for three crystals). The powder X-ray diffraction (PXRD) pattern of the bulk material from the electrocrystalliation of **2**, (**Figure S18**), is consistent with the simulated spectrum for the single-crystal X-ray structure of **2**.s

Electrochemical characterization: Cyclic voltammetry experiments were recorded using a Hokuto Denko HZ-5000 Automatic Polarization System. The instrument was fitted with a three-electrode system consisting of a Pt disk as the working electrode, a Pt wire as the auxiliary electrode and an Ag/AgCl in 3 M NaCl solution as the reference electrode. Experiments were conducted at room temperature in dry DMF solution with *n*-$BuNBF_4$ (0.1 M) as the supporting electrolyte. Cyclic voltammetry experiments were conducted at a scan rate of 200 mV/s, unless otherwise specified. Each solution was purged with N_2 prior to the experiment. Ferrocene (Fc) was used as the internal standard in each measurement.

Optical characterisation: UV-vis solution absorption measurements were recorded using a Jasco V-670 UV/vis/NIR spectrophotometer controlled with SpectraManager software. Solution state UV-visible absorption spectra were obtained using freshly prepared solutions of the complexes in CH_2Cl_2 at low concentrations ($<10^{-5}$ M) in a 1 cm pathlength cell. Baseline correction was achieved by reference to pure solvent in the same cuvette.

XRD characterization: Powder X-ray diffraction studies were performed using a Rigaku SmartLab using Cu-Kα radiation. For the single crystal data of complex **NBu_4·[*trans*-1]**, a suitable crystal [0.17×0.15×0.04 mm^3] was selected and mounted on a MITIGEN holder in Paratone oil on a Rigaku Oxford Diffraction SuperNova diffractometer (Cu-Kα radiation λ = 1.54184 Å). The crystal of **NBu_4·[*trans*-1]** was kept at T = 120.0 K during data collection. Four distinctly separate twin domains of the measured crystal were identified by using CrysAlisPro.[83] The structure of **NBu_4·[*trans*-1]** was solved with the SHELXT[84] structure solution program using the Intrinsic Phasing solution method and by using Olex2[85] as the graphical interface. The model of **NBu_4·[*trans*-1]** was refined with version 2016/6 of SHELXL[86] using Least Squares minimisation. One of the *n*-butyl chains was modelled as disordered over two sites, consistent with very large displacement ellipsoids. The disordered *n*-butyl chain was refined with restraints on the anisotropic displacement parameters (RIGU restrain), and constraints on the anisotropic displacement parameters (EADP constraint) and coordinates (EXYZ constraint). For the single crystal data of complex **2**, a suitable crystal [0.16×0.07×0.02 mm^3] was

selected and mounted on a loop in oil (CryoLoop, Immersion Oil, Type B; Hampton Research Corp.) on a Rigaku RA-Micro007 with a Saturn CCD detector (graphite-monochromated Mo-Kα radiation λ = 0.710690 Å) under a cold nitrogen stream. The crystal of **2** was kept at T = 123 K during data collection. The frame data were integrated and corrected for absorption with the Rigaku/MSC CrystalClear package.[87] The structure of **2** was solved by direct method (SIR92[88]) and standard difference map techniques, and were refined with full-matrix least-square procedures on F^2. All calculations for **2** were performed using the crystallographic software package, Crystal Structure,[89] except for refinement. The model of **2** was refined with version 2016/4 of SHELXL[86] using Least Squares minimisation. Anisotropic refinement was applied to all non-hydrogen atoms, and all hydrogen atoms were placed at calculated positions and refined using a riding model for both crystals. CCDC 1908634 and 1908635 contain the supplementary crystallographic data for this paper. This data can be obtained free of charge from The Cambridge Crystallographic Data Centre via www.ccdc.cam.ac.uk/data_request/cif.

Magnetic Characterisation: Magnetic susceptibility measurements were performed on polycrystalline samples from 2 to 300 K using a Quantum Design Magnetic Property Measurement System (MPMS)-XL SQUID magnetometer with MPMS MultiVu Application software to process the data. The magnetic field used was 3 T. The paramagnetic susceptibility χ_p was calculated by correction with the diamagnetic contributions from the sample (Pascal's constants: -3.13×10^{-4} emu mol^{-1} [90]) and holder (a plastic straw) and the contribution from the ferromagnetic impurity.

Computational details: DFT calculations for isolated molecular systems were performed using the Gaussian03 package by using the molecular geometry in the crystal structure of **2**. The calculations were carried out using the hybrid B3LYP functional, with the 6-31G* basis sets for H, C, and S, and the LanL2DZ basis set and Los Alamos effective core potentials for Au. The intermolecular transfer integrals and tight-binding band structure calculations were of the extended Hückel type, and made using the Caesar 2.0.[91] The modified Wolfsberg-Helmholtz formula was used to calculate the nondiagonal matrix elements of the Hamiltonian.[92] All valence electrons were taken into account in the calculations, and the basis set consisted of Slater-type orbitals of double-ζ quality for Au 5d and S 3s

and 2p, and of single-ζ quality for Au 6s and 6p, C 2s and 2p and H 1s. The ionization potentials, contraction coefficients, and exponents were taken from previous work, implemented in Caesar 2.0.

Intermolecular hopping carrier mobilities were calculated on the basis of Marcus theory.[78–81] First, intermolecular electronic coupling matrix elements (V_{ab}) were calculated as follows:

$$V_{ab} = \frac{H_{ab} - \frac{S_{ab}(H_{aa} - H_{bb})}{2}}{1 - S_{ab}^2}$$

where H_{ab} = intermolecular charge transfer integrals, S_{ab} = overlap integrals and H_{aa} and H_{bb} = the energies of the two molecular orbitals. These were calculated as described for the band structure calculations.

Then the intermolecular charge transfer rate constants (k_{ET}) were calculated as follows:

$$k_{ET} = \frac{V_{ab}^2}{h}\left(\frac{\pi}{\lambda k_B T}\right)^{1/2} e^{\left(\frac{-\lambda}{4k_B T}\right)}$$

where h, k_B, and T are Planck's constant, Boltzmann constant, and temperature, respectively. The reorganization energies upon intermolecular hole (or electron) transfer (λ) were obtained from:

$$\lambda = (E_+^* - E_+) + (E^* - E)$$

where E, E_+, E^*, and E_+^* are the energies for an optimised neutral molecule, optimised cation (anion, E_-) molecule, neutral state on cation (anion) structure, and cation (anion) state on neutral structure, respectively. These were calculated at the B3LYP/LANL2DZ/6-31G* level using the Gaussian16 package.

Intermolecular hopping mobilities (μ) were estimated as follows:

$$\mu_{hopping} = \frac{ed^2}{k_B T} k_{ET}$$

where d is the intermolecular center-to-center distance of adjacent molecules.

As described in the manuscript, the optimised structures were calculated by two methods; the first involved restricting the dihedral angles between the dithiolene and benzene rings and between the

benzene rings to fit with geometry observed in the crystal structure. These results are shown in Tables 5, S6-7. The second method allowed full optimisation of the molecular geometries, this resulted in large deviations from the geometry present in the crystal structure, even for the neutral molecule. The results of these calculations are shown in Tables S8-10 .

Single Crystal Conductivity Measurements: The temperature dependence of the conductivity of **2** was measured on single crystals with a two-probe method using a Quantum Design Physical Property Measurement System (PPMS) and an Advantest R6245 2 Channel Voltage Current Source/Monitor. The conductivity was measured in the *ab* plane and along the *c* axis of the crystal by applying a constant voltage of 1 V. Gold wires were attached to the crystals with a gold paste.

Single-crystal Field-Effect Transistors: Single-crystal field-effect transistors were prepared by gluing gold wires (source and drain) to a single crystal of **2** in the *ab* plane, followed by deposition of Parylene C as a dielectric layer (790 nm, determined by UV-vis spectroscopy). Gold paste was then spread over the Parylene-C layer, and a gold wire glued to the surface to form the gate electrode. The field effect mobility μ is estimated by:

$$\mu = \left|\frac{\partial I_D}{\partial V_G}\right| \frac{L}{V_D W C_i}$$

where L, W, and C_i are the channel length (130 μm), channel width (210 μm), and dielectric layer capacitance per unit area (3.6 nF/cm^2), respectively. An activation energy E_a for the thermal-activated behaviour of the field effect mobility is calculated by:

$$\mu = \mu_0 \exp\left(-\frac{E_a}{k_B T}\right)$$

Supporting Information

X-ray crystallographic files of **NBu$_4$·[*trans*-1]** and **2** in CIF format. Solution ^{1}H NMR, UV-Vis data and cyclic voltammograms of **NBu$_4$·[*trans*-1]**. UV-vis spectroscopy, solid-state ^{1}H NMR, heat capacity measurements, low-temperature X-ray analysis, EPR measurements and further FET measurements are available for complex **2**. This material is available via Wiley Online Library.

Acknowledgments

The authors thank Dr. Gary Nichol for the crystallographic data collection and refinement; The University of Edinburgh for funding the diffractometer purchase. The authors thank the Leverhulme Trust (RPG-2016-152), the Japan Society for the Promotion of Science (JSPS) KAKENHI Grants (nos. JP16H06353 and JP18H04482), and the JSPS Bilateral Collaboration and Core-to-Core Program (A. Advanced Research Networks) for financial support. This work was partly supported by Nanotechnology Platform Program (Molecule and Material Synthesis) of the Ministry of Education, Culture, Sports, Science and Technology (MEXT), Japan. The authors also thank Mr. Yoshinori Okano in Institute for Molecular Science for his support of the low-temperature X-ray analysis.

Author Contributions

‡A.M. and H.B. contributed equally to this work.

Notes

The authors declare no competing financial interest.

Received: ((will be filled in by the editorial staff))
Revised: ((will be filled in by the editorial staff))
Published online: ((will be filled in by the editorial staff))

References

[1] R. Kato, *Chem. Rev.* **2004**, *104*, 5319.

[2] D. G. Branzea, F. Pop, P. Auban-Senzier, R. Clérac, P. Alemany, E. Canadell, N. Avarvari, *J. Am. Chem. Soc.* **2016**, *138*, 6838.

[3] J. P. M. Nunes, M. J. Figueira, D. Belo, I. C. Santos, B. Ribeiro, E. B. Lopes, R. T. Henriques, J. Vidal-Gancedo, J. Veciana, C. Rovira, M. Almeida, *Chem. - A Eur. J.* **2007**, *13*, 9841.

[4] N. Tenn, N. Bellec, O. Jeannin, L. Piekara-Sady, P. Auban-Senzier, J. Íñiguez, E. Canadell, D. Lorcy, *J. Am. Chem. Soc.* **2009**, *131*, 16961.

[5] W. Suzuki, E. Fujiwara, A. Kobayashi, Y. Fujishiro, E. Nishibori, M. Takata, M. Sakata, H. Fujiwara, H. Kobayashi, *J. Am. Chem. Soc.* **2003**, *125*, 1486.

[6] B. Zhou, M. Shimamura, E. Fujiwara, A. Kobayashi, T. Higashi, E. Nishibori, M. Sakata, Cui, K. Takahashi, H. Kobayashi, *J. Am. Chem. Soc.* **2006**, *128*, 3872.

[7] Y. Le Gal, T. Roisnel, P. Auban-Senzier, N. Bellec, J. Íñiguez, E. Canadell, D. Lorcy, *J. Am. Chem. Soc.* **2018**, *140*, 6998.

[8] P. Stoliar, P. Diener, J. Tranchant, B. Corraze, B. Brière, V. Ta-Phuoc, N. Bellec, M. Fourmigué, D. Lorcy, E. Janod, L. Cario, *J. Phys. Chem. C* **2015**, *119*, 2983.

[9] H. Tanaka, S. Hara, M. Tokumoto, A. Kobayashi, H. Kobayashi, *Chem. Lett.* **2007**, *36*, 1006.

[10] B. Zhou, H. Yajima, Y. Idobata, A. Kobayashi, T. Kobayashi, E. Nishibori, H. Sawa, H. Kobayashi, *Chem. Lett.* **2012**, *41*, 154.

[11] S. Ishibashi, H. Tanaka, M. Kohyama, M. Tokumoto, A. Kobayashi, H. Kobayashi, K. Terakura, *J. Phys. Soc. Japan* **2005**, *74*, 843.

[12] Y. Le Gal, T. Roisnel, P. Auban-Senzier, T. Guizouarn, D. Lorcy, *Inorg. Chem.* **2014**, *53*, 8755.

[13] M. Sasa, E. Fujiwara, A. Kobayashi, S. Ishibashi, K. Terakura, Y. Okano, H. Fujiwara, H. Kobayashi, *J. Mater. Chem.* **2005**, *15*, 155.

[14] K. Mebrouk, W. Kaddour, P. Auban-Senzier, C. Pasquier, O. Jeannin, F. Camerel, M. Fourmigué, *Inorg. Chem.* **2015**, *54*, 7454.

[15] Y. Hara, K. Miyagawa, K. Kanoda, M. Shimamura, B. Zhou, A. Kobayashi, H. Kobayashi, *J. Phys. Soc. Japan* **2008**, *77*, 53706.

[16] G. Yzambart, N. Bellec, G. Nasser, O. Jeannin, T. Roisnel, M. Fourmigué, P. Auban-Senzier, J. Íñiguez, E. Canadell, D. Lorcy, *J. Am. Chem. Soc.* **2012**, *134*, 17138.

[17] A. Filatre-Furcate, N. Bellec, O. Jeannin, P. Auban-Senzier, M. Fourmigué, J. Íñiguez, E. Canadell, B. Brière, V. Ta Phuoc, D. Lorcy, J. Íniguez, E. Canadell, B. Brière, V. Ta Phuoc, D. Lorcy, J. Íñiguez, E. Canadell, B. Brière, V. Ta Phuoc, D. Lorcy, *Inorg. Chem.* **2016**, *55*, 6036.

[18] R. Le Pennec, O. Jeannin, P. Auban-Senzier, M. Fourmigué, *New J. Chem.* **2016**, *40*, 7113.

[19] S. Kokatam, K. Ray, J. Pap, E. Bill, W. E. Geiger, R. J. LeSuer, P. H. Rieger, T. Weyhermüller, F. Neese, K. Wieghardt, *Inorg. Chem.* **2007**, *46*, 1100.

[20] N. C. Schiødt, T. Bjørnholm, K. Bechgaard, J. J. Neumeier, C. Allgeier, C. S. Jacobsen, N. Thorup, *Phys. Rev. B* **1996**, *53*, 1773.

[21] O. J. Dautel, M. Fourmigué, E. Canadell, P. Auban-Senzier, *Adv. Funct. Mater.* **2002**, *12*, 693.

[22] A. Filatre-Furcate, T. Roisnel, M. Fourmigué, O. Jeannin, N. Bellec, P. Auban-Senzier, D. Lorcy, *Chem. - A Eur. J.* **2017**, *23*, 16004.

[23] A. A. Leitch, K. Lekin, S. M. Winter, L. E. Downie, H. Tsuruda, J. S. Tse, M. Mito, S. Desgreniers, P. A. Dube, S. Zhang, Q. Liu, C. Jin, Y. Ohishi, R. T. Oakley, *J. Am. Chem. Soc* **2011**, *133*, 6051.

[24] A. Mailman, S. M. Winter, X. Yu, C. M. Robertson, W. Yong, J. S. Tse, R. A. Secco, Z. Liu, P. A. Dube, J. A. K. Howard, R. T. Oakley, *J. Am. Chem. Soc.* **2012**, *134*, 9886.

[25] B. Brière, J. Caillaux, Y. Le Gal, D. Lorcy, S. Lupi, A. Perucchi, M. Zaghrioui, J. C. Soret, R. Sopracase, V. Ta Phuoc, *Phys. Rev. B* **2018**, *97*, 035101.

[26] M. Bousseau, L. Valade, J. P. Legros, P. Cassoux, M. Garbauskas, L. V Interrante, *J. Am. Chem. Soc.* **1986**, *108*, 1908.

[27] L. Brossard, M. Ribault, L. Valade, P. Cassoux, *Phys. B+C* **1986**, *143*, 378.

[28] S. Ishibashi, K. Terakura, A. Kobayashi, *J. Phys. Soc. Japan* **2008**, *77*, 024702.

[29] M. Tsuchiizu, Y. Omori, Y. Suzumura, M.-L. Bonnet, V. Robert, *J. Chem. Phys.* **2012**, *136*, 044519.

[30] D. Belo, H. Alves, E. Branco Lopes, M. T. Duarte, V. Gama, R. Teives Henriques, M. Almeida, A. Pérez-Benítez, C. Rovira, J. Veciana, *Chemistry (Easton).* **2001**, *7*, 511.

[31] G. Rindorf, N. Thorup, T. Bjørnholm, K. Bechgaard, *Acta Crystallogr. Sect. C Cryst. Struct. Commun.* **1990**, *46*, 1437.

[32] N. C. Schiodt, P. Sommer-Larsen, T. Bjornholm, M. F. Nielsen, J. Larsen, K. Bechgaard, *Inorg. Chem.* **1995**, *34*, 3688.

[33] M. A. Mazid, M. T. Razi, P. J. Sadler, *Inorg. Chem.* **1981**, *20*, 2872.

[34] R. Perochon, L. Piekara-Sady, W. Jurga, R. Clérac, M. Fourmigué, *Dalt. Trans.* **2009**, *0*, 3052.

[35] G. C. Papavassiliou, G. C. Anyfantis, N. Ioannidis, V. Petrouleas, P. Paraskevopoulou, C. P. Raptopoulou, V. Psycharis, N. Ioannidis, V. Petrouleas, P. Paraskevopoulou, *Polyhedron* **2009**, *28*, 3368.

[36] R. Perochon, P. Davidson, S. Rouzière, F. Camerel, L. Piekara-Sady, T. Guizouarn, M. Fourmigué, *J. Mater. Chem.* **2011**, *21*, 1416.

[37] A. J. Schultz, H. H. Wang, L. C. Soderholm, T. L. Sifter, J. M. Williams, K. Bechgaard, M.-H. H. Whangbo, *Inorg. Chem.* **1987**, *26*, 3757.

[38] G.-E. Matsubayashi, A. Yokozawa, *J. Chem. Soc., Dalt. Trans.* **1990**, 3535.

[39] J. M. Tunney, A. J. Blake, E. S. Davies, J. McMaster, C. Wilson, C. D. Garner, *Polyhedron* **2006**, *25*, 591.

[40] S. Rabaça, A. C. Cerdeira, S. Oliveira, I. C. Santos, R. T. Henriques, L. C. J. Pereira, J. T. Coutinho, M. Almeida, *Polyhedron* **2012**, *39*, 91.

[41] R. Perochon, C. Poriel, O. Jeannin, L. Piekara-Sady, M. Fourmigué, *Eur. J. Inorg. Chem.* **2009**, *2009*, 5413.

[42] A. Filatre-Furcate, P. Auban-Senzier, M. Fourmigué, T. Roisnel, V. Dorcet, D. Lorcy, *Dalt. Trans.* **2015**, *44*, 15683.

[43] T. Higashino, O. Jeannin, T. Kawamoto, D. Lorcy, T. Mori, M. Fourmigué, *Inorg. Chem.* **2015**, *54*, 9908.

[44] T. D. Anthopoulos, G. C. Anyfantis, G. C. Papavassiliou, D. M. de Leeuw, *Appl. Phys. Lett.* **2007**, *90*, 122105.

[45] E. C. P. Smits, T. D. Anthopoulos, S. Setayesh, E. Van Veenendaal, R. Coehoorn, P. W. M. Blom, B. De Boer, D. M. De Leeuw, *Phys. Rev. B* **2006**, *73*, 205316.

[46] T. D. Anthopoulos, S. Setayesh, E. Smits, M. Cölle, E. Cantatore, B. de Boer, P. W. M. Blom, D. M. de Leeuw, *Adv. Mater.* **2006**, *18*, 1900.

[47] K. Sakai, T. Hasegawa, M. Ichikawa, Y. Taniguchi, *Chem. Lett.* **2006**, *35*, 302.

[48] L. Qu, Y. Guo, H. Luo, C. Zhong, G. Yu, Y. Liu, J. Qin, *Chem. Commun.* **2012**, *48*, 9965.

[49] S. Noro, T. Takenobu, Y. Iwasa, H.-C. Chang, S. Kitagawa, T. Akutagawa, T. Nakamura, *Adv. Mater.* **2008**, *20*, 3399.

[50] T. Fujimoto, M. M. Matsushita, K. Awaga, *J. Phys. Chem. C* **2013**, *117*, 31.

[51] G. C. Papavassiliou, G. C. Anyfantis, G. A. Mousdis, *Crystals* **2012**, *2*, 762.

[52] S. Dalgleish, J. G. Labram, Z. Li, J. Wang, C. R. McNeill, T. D. Anthopoulos, N. C. Greenham, N. Robertson, *J. Mater. Chem.* **2011**, *21*, 15422.

[53] A. Sugimori, N. Tachiya, M. Kajitani, T. Akiyama, *Organometallics* **1996**, *15*, 5664.

[54] O. Jeannin, J. Delaunay, F. Barrière, M. Fourmigué, *Inorg. Chem.* **2005**, *44*, 9763.

[55] K. Ray, T. Weyhermüller, A. Goossens, M. W. J. Crajé, K. Wieghardt, *Inorg. Chem.* **2003**, *42*, 4082.

[56] L. Ambrosio, M. C. Aragoni, M. Arca, F. A. Devillanova, M. B. Hursthouse, S. L. Huth, F. Isaia, V. Lippolis, A. Mancini, A. Pintus, *Chem. - An Asian J.* **2010**, *5*, 1395.

[57] M. C. Aragoni, M. Arca, F. A. Devillanova, F. Isaia, V. Lippolis, A. Pintus, *Chem. - An Asian J.* **2011**, *6*, 198.

[58] R. Eisenberg, H. B. Gray, *Inorg. Chem.* **2011**, *50*, 9741.

[59] J. A. McCleverty, in *Prog. Inorg. Chem.*, **2007**, pp. 49–221.

[60] Y. Yoshida, H. Ito, M. Maesato, Y. Shimizu, H. Hayama, T. Hiramatsu, Y. Nakamura, H. Kishida, T. Koretsune, C. Hotta, G. Saito, *Nat. Phys.* **2015**, *11*, 679.

[61] K. Miyagawa, A. Kawamoto, Y. Nakazawa, K. Kanoda, *Phys. Rev. Lett.* **1995**, *75*, 1174.

[62] L. Li, Q. Tang, H. Li, X. Yang, W. Hu, Y. Song, Z. Shuai, W. Xu, Y. Liu, D. Zhu, *Adv. Mater.* **2007**, *19*, 2613.

[63] X. Shao, S. Wang, X. Li, Z. Su, Y. Chen, Y. Xiao, *Dye. Pigment.* **2016**, *132*, 378.

[64] H. Wang, F. Zhu, J. Yang, Y. Geng, D. Yan, *Adv. Mater.* **2007**, *19*, 2168.

[65] R. W. I. de Boer, A. F. Stassen, M. F. Craciun, C. L. Mulder, A. Molinari, S. Rogge, A. F. Morpurgo, *Appl. Phys. Lett.* **2005**, *86*, 262109.

[66] X. Zhang, Y. Chen, *Inorg. Chem. Commun.* **2014**, *39*, 79.

[67] X. Kong, G. Lu, X. Zhang, X. Li, Y. Chen, J. Jiang, *Dye. Pigment.* **2017**, *143*, 203.

[68] T. Hasegawa, K. Mattenberger, J. Takeya, B. Batlogg, *Phys. Rev. B* **2004**, *69*, 245115.

[69] M. Sakai, H. Sakuma, Y. Ito, A. Saito, M. Nakamura, K. Kudo, *Phys. Rev. B* **2007**, *76*, 045111.

[70] Y. Kawasugi, H. M. Yamamoto, N. Tajima, T. Fukunaga, K. Tsukagoshi, R. Kato, *Phys. Rev. B* **2011**, *84*, 125129.

[71] J.-Y. Cho, B. Domercq, S. C. Jones, J. Yu, X. Zhang, Z. An, M. Bishop, S. Barlow, S. R. Marder, B. Kippelen, *J. Mater. Chem.* **2007**, *17*, 2642.

[72] T. Taguchi, H. Wada, T. Kambayashi, B. Noda, M. Goto, T. Mori, K. Ishikawa, H. Takezoe, *Chem. Phys. Lett.* **2006**, *421*, 395.

[73] C. Pearson, J. E. Gibson, M. C. Petty, A. J. Moore, M. R. Bryce, *Electron. Lett.* **1993**, *29*, 1377.

[74] L. Pilia, M. M. Matsushita, K. Awaga, N. Robertson, *New J. Chem.* **2017**, *41*, 5487.

[75] S.-I. Noro, H.-C. Chang, T. Takenobu, Y. Murayama, T. Kanbara, T. Aoyama, T. Sassa, T. Wada, D. Tanaka, S. Kitagawa, Y. Iwasa, T. Akutagawa, T. Nakamura, *J. Am. Chem. Soc.* **2005**, *127*, 10012.

[76] Y. Takahashi, T. Hasegawa, Y. Abe, Y. Tokura, K. Nishimura, G. Saito, *Appl. Phys. Lett.* **2005**, *86*, 063504.

[77] Y. Miyoshi, K. Takahashi, T. Fujimoto, H. Yoshikawa, M. M. Matsushita, Y. Ouchi, M. Kepenekian, V. Robert, M. P. Donzello, C. Ercolani, K. Awaga, *Inorg. Chem* **2012**, *51*, 11.

[78] Y. Xie, T. Fujimoto, S. Dalgleish, Y. Shuku, M. M. Matsushita, K. Awaga, *J. Mater. Chem. C* **2013**, *1*, 3467.

[79] K. Senthilkumar, F. C. Grozema, C. F. Guerra, F. M. Bickelhaupt, F. D. Lewis, Y. A. Berlin, M. A. Ratner, L. D. A. Siebbeles, *J. Am. Chem. Soc.* **2005**, *127*, 14894.

[80] K. Senthilkumar, F. C. Grozema, F. M. Bickelhaupt, L. D. A. Siebbeles, *J. Chem. Phys.* **2003**, *119*, 9809.

[81] M. D. Newton, *Chem. Rev.* **1991**, *91*, 767.

[82] A. K. Bhattacharya, A. G. Hortmann, *J. Org. Chem.* **1974**, *39*, 95.

[83] CrysAlisPro Software System, Oxford Diffraction /Agilent Technologies UK Ltd, Yarnton, England. **2015**.

[84] G. M. Sheldrick, *Acta Crystallogr. Sect. A Found. Adv.* **2015**, *71*, 3.

[85] O. V. Dolomanov, L. J. Bourhis, R. J. Gildea, J. A. K. Howard, H. Puschmann, *J. Appl. Crystallogr.* **2009**, *42*, 339.

[86] G. M. Sheldrick, IUCr, *Acta Crystallogr. Sect. C Struct. Chem.* **2015**, *71*, 3.

[87] CrystalClear: Data Collection and Processing Software. Rigaku Corporation (1998-2015). Tokyo 196-8666, Japan.

[88] A. Altomare, G. Cascarano, C. Giacovazzo, A. Guagliardi, *Completion and Refinement of Crystal Structures with SIR92*, **1993**.

[89] CrystalStructure 4.2.5: Crystal Structure Analysis Package. Rigaku Corporation (2000-2017). Tokyo 196-8666, Japan.

[90] G. A. Bain, J. F. Berry, *J. Chem. Educ.* **2008**, *85*, 532.

[91] J. Ren, W. Liang, M.-H. Whangbo, **1998**.

[92] J. H. Ammeter, H.-B. Bürgi, J. C. Thibeault, R. Hoffmann, *Counterintuitive Orbital Mixing in Semiempirical and Ab Initio Molecular Orbital Calculations*, **1978**.

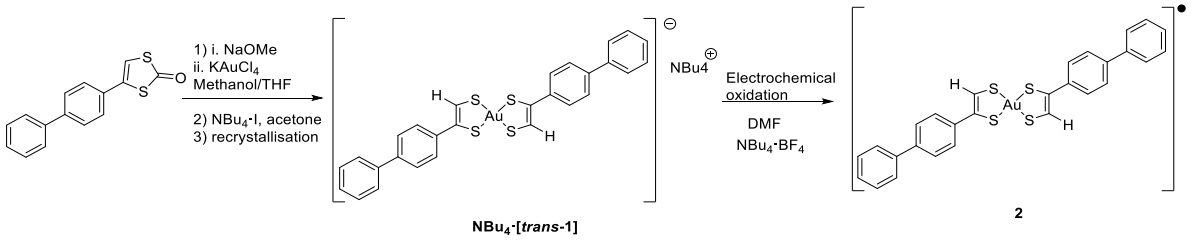

Scheme 1. Synthesis of **2**.

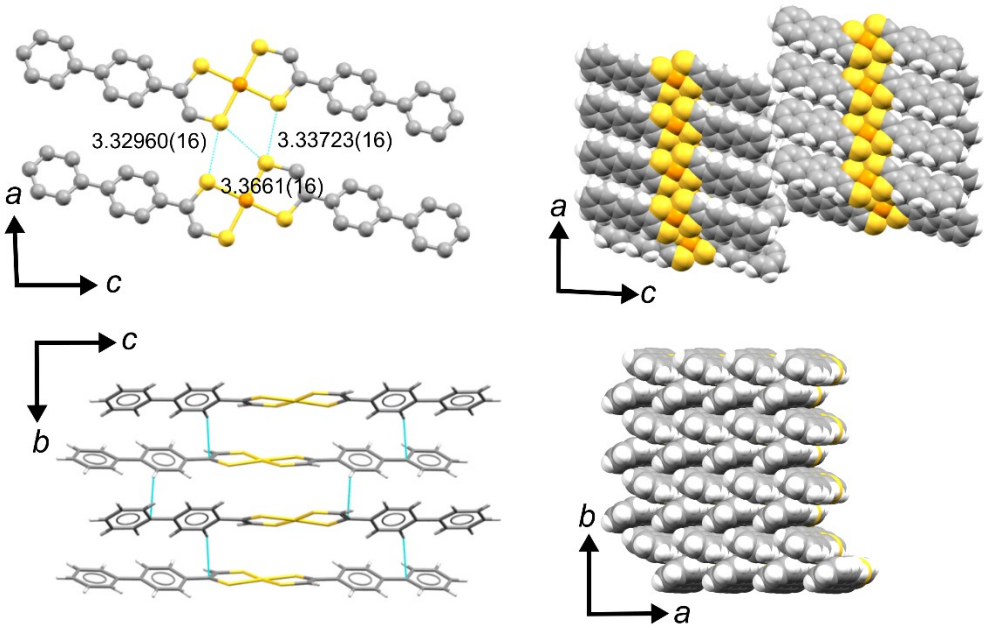

Figure 1. Crystal structure of the neutral gold complex **2**.

Table 1. Crystallographic data for complex **2**.

Formula	$C_{28}H_{20}AuS_4$
Formula weight / g mol^{-1}	681.67
Temperature / K	123
Crystal dimensions / mm^3	0.16 × 0.07 × 0.02
System	Monoclinic
Space group	$P2_1/c$ (#14)
a / Å	6.1872(16)
b / Å	7.2049(18)
c / Å	51.832(13)
β/°	92.775(2)
V / Å^3	2307.9(10)
Z	4
ρ_{calcd} / g cm^{-3}	1.962
μ (MoKα) / cm^{-1}	67.751
λ / Å	0.71075
$2\theta_{max}$ / °	54.9
Reflections collected	16118
Unique reflections (R_{int})	5089 (0.0527)
Number of parameters	298
Final R_1 [$I > 2\sigma(I)$]	0.0349
wR_2 (all data)	0.0595
Goodness of fit	1.021
Residual electron density / Å^{-3}	1.32 e$^-$

Table 2. Bond lengths of the dithiolene moieties of **2**.

Bond	Bond length [Å]			
Au-S	2.2930(12)	2.3009(12)	2.3001(15)	2.3087(15)
C-S	1.712(4)	1.759(4)	1.693(4)	1.727(4)

C-C	1.367(5)	1.348(6)

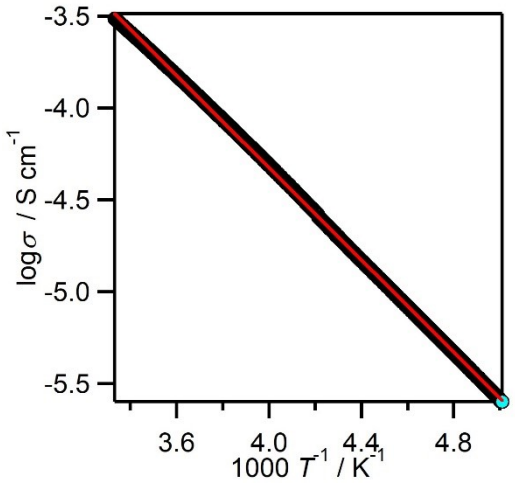

Figure 2. Temperature dependence of the conductivity for **2** in the temperature range of 200–300 K in the *ab* plane. The red line indicates the theoretical fit with an activation energy of 0.11 eV.

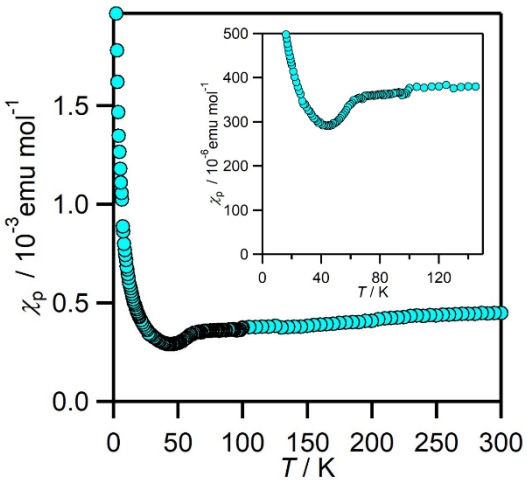

Figure 3. Temperature dependence of the paramagnetic susceptibility for the neutral gold complex **2** in the temperature range of 2–300 K. The inset shows an expanded view of the data.

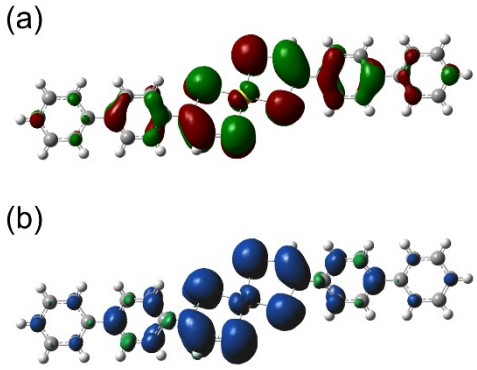

Figure 4. SOMO (a, isocontour value of 0.02 au) and spin density distribution (b, isocontour value of 0.0004 au) of the neutral gold complex **2.**

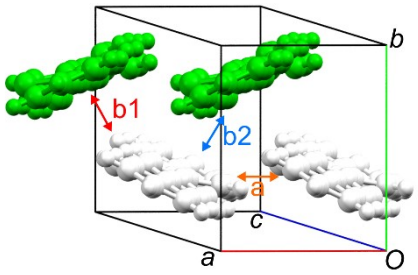

Figure 5. Definition of the intermolecular interactions in the crystal structure of **2**.

Table 3. Estimated overlap integrals and transfer integrals in the crystal structure of **2**.

Interaction	*S* [meV]	*t* [meV]
a	-0.9	20.6
b1	-6.8	168.8
b2	14.0	-315.9

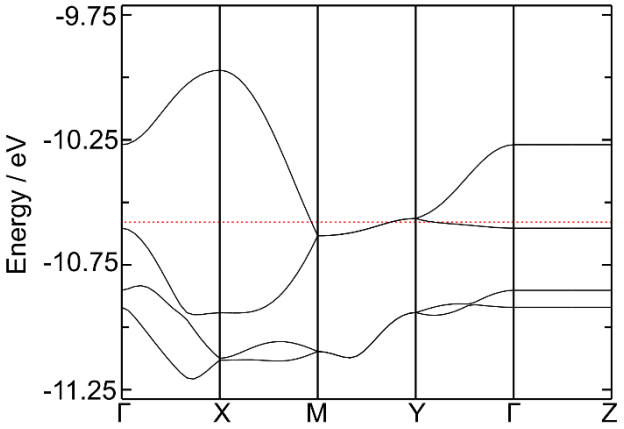

Figure 6. Calculated (tight binding) band structure of **2** with the SOMO-1 (4 bands, each line represents two bands) and SOMO (4 bands, each line represents two bands) bands represented. The LUMO bands are significantly higher in energy and are not shown. The points in reciprocal space that are represented are Γ = (0,0,0), X = (1/2,0,0), M = (1/2,1/2,0), Y = (0,1/2,0), Z = (0,0,1/2). The dotted line represents the Fermi level, assuming metallic filling of the bands.

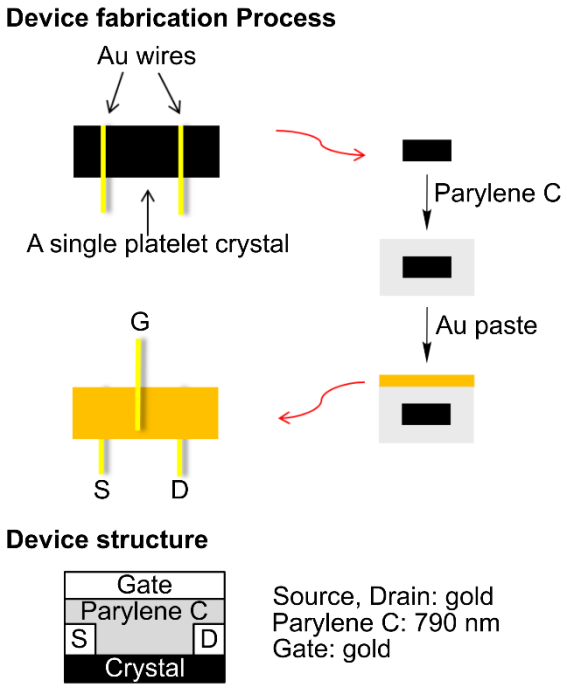

Figure 7. Schematic image of the device fabrication process (top) and device structure (bottom).

Table 4. Reported electron and hole mobilities for a selection of metal complexes.[i]

Complex	μ_e / cm^2 V^{-1} s^{-1}	μ_h / cm^2 V^{-1} s^{-1}	Reference
Ni(dpedt)(dmit)	3 x 10^{-4}	10^{-4}	[44,51]
NiDT	10^{-3}	10^{-3}	[46]
Ni(mi-5edt)$_2$	10^{-6}	10^{-7}	[51]
Ni(tmedt)(dddt)	0.02-0.045	0.02	[51]
Ni(dpedt)(dddt)	3 x 10^{-4}	3 x 10^{-4}	[51]
$(NO)_x$Ni(dmit)	0.18	-	[51]
Ni(tfpdt)$_2$	0.11	-	[48]
Ni[$C_6H_4(NH)_2$]$_2$	1.6 x 10^{-3}	4.3 x 10^{-3}	[49]

$Ni[C_7H_6(NH)_2]_2$	1.3 x 10^{-3}	1.7 x 10^{-2}	[49]
$Pt(bqd)_2$	0.2	-	[47]
PbPc	10^{-3}	10^{-2}	[50]
TiOPc	10^{-3}	10^{-3}	[50]
	-	10	[62]
$F_{12}CuPc$	0.006	0.005	[63]
ZnPc	-	0.32	[64]
CuPc	10^{-3}	0.3	[65]
FePc	0.03	0.3	[65]
$(TPP)Eu_2[Pc(OPh)_8]_2$	0.08	0.04	[66]
$Eu_2[Pc(ONh)_8]_3$	0.06	0.11	[67]

i) Numerous phthalocyanine complexes have been studied in OFETs.[62] For the sake of brevity, only those with the highest values, or with reported ambipolar behavior, are included.

Table 5. Calculated intermolecular transfer integrals (H_{ab}), overlap intergrals (S_{ab}), center-to-center distances (d), orbital interaction energy (V), reorganization energy (λ) and electron and hole hopping mobilities ($\mu_{hopping}$) for each interaction in crystalline **2**.

Carrier	Interaction[a)]	H_{ab}[b)] [eV]	S_{ab}[b)] [meV]	d [Å]	V [eV]	λ[b)] [eV]	$\mu_{hopping}$ [$cm^2V^{-1}s^{-1}$]
hole	b1	-0.169	6.8	5.545	-0.095	0.147	1.82
hole	a	-0.021	0.9	6.187	-0.011	0.147	0.03
hole	b2	0.316	-14.0	4.829	0.165	0.147	4.12
electron	b1	-0.169	6.8	5.545	-0.095	0.113	2.87
electron	a	-0.021	0.9	6.187	-0.011	0.113	0.05
electron	b2	0.316	-14.0	4.829	0.165	0.113	6.50

[a)] Corresponding molecular contacts are indicated in Fig 5. [b)] Calculated at the B3LYP/LANL2DZ/6-31G* level.

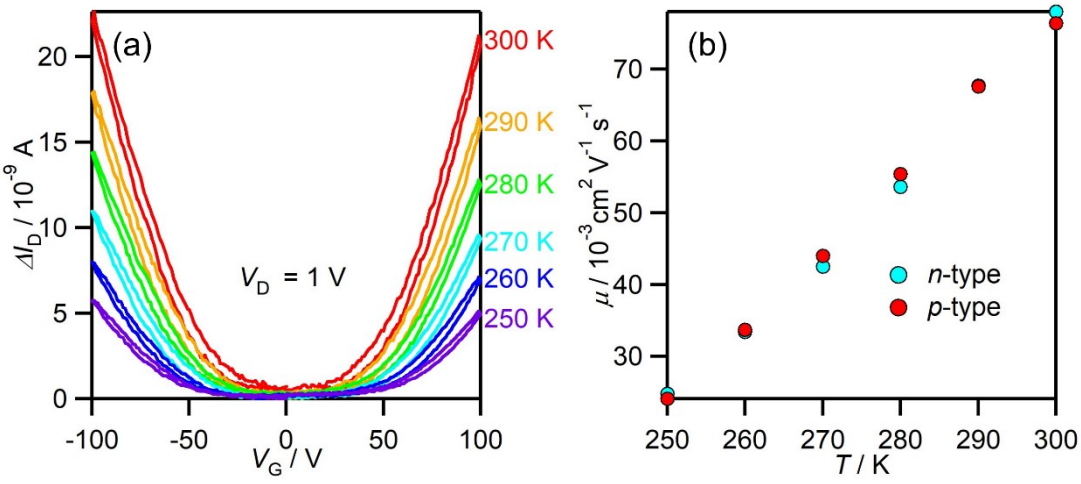

Figure 8. Temperature dependence of the transfer characteristics (a) and field effect mobility (b) for a SC-FET of **2**.

High ambipolar mobilities: A new neutral gold dithiolene complex is synthesised, and its electronic properties investigated by conductivity measurement and band structure calculations. Single crystal field effect transistors (FETs) are fabricated, showing incredibly well balanced ambipolar behaviour, with high charge carrier mobilities of 0.078 $cm^2 V^{-1} s^{-1}$, the highest ambipolar mobilities reported for metal dithiolene complexes.

Keywords: charge transport, field-effect transistors, organic semiconductors, dithiolene ligands, gold

Asato Mizuno, Helen Benjamin, Yasuhiro Shimizu, Yoshiaki Shuku,a Michio M. Matsushita, Neil Robertson*, and Kunio Awaga*

High ambipolar mobility in a neutral radical gold dithiolene complex